1 **Short summary.** Wolverine denning habitat inferred using a snow threshold differed for three different spatial
2 representations of snow. These differences were based on the annual volume of snow and the elevation of the snow
3 line. While denning habitat was most influenced by winter meteorological conditions, our results show that studies
4 applying thresholds to environmental datasets should report uncertainties stemming from different spatial
5 resolutions and uncertainties introduced by the thresholds themselves.

6 # Interactions between thresholds and spatial discretizations of snow: insights
7 # from estimates of wolverine denning habitat in the Colorado Rocky
8 # Mountains

9 Justin M. Pflug[1,a,b], Yiwen Fang[2], Steven A. Margulis[2], Ben Livneh[1,3]

10 [1]Cooperative Institute for Research in Environmental Science (CIRES), University of Colorado,
11 Boulder, CO, 80309, USA
12 [2]Department of Civil and Environmental Engineering, University of California, Los Angeles, CA,
13 90095, USA
14 [3]Department of Civil, Environmental and Architectural Engineering, University of Colorado, Boulder,
15 CO, 80309, USA
16 [a]now at: Hydrological Sciences Laboratory, NASA Goddard Space Flight Center, Greenbelt, MD,
17 20771, USA
18 [b]now at: ESSIC, University of Maryland, College Park, College Park, MD, 20742, USA

19 *Correspondence to*: Justin M. Pflug (jpflug@umd.edu)

20 **Abstract.** Thresholds can be used to interpret environmental data in a way that is easily communicated and useful
21 for decision making purposes. However, thresholds are often developed for specific data products and time periods,
22 changing findings when the same threshold is applied to datasets or periods with different characteristics. Here, we
23 test the impact of different spatial discretizations of snow on annual estimates of wolverine denning opportunities in
24 the Colorado Rocky Mountains, defined using a snow water equivalent (SWE) threshold (0.20 m) and threshold date
25 (15 May) from previous habitat assessments. Annual potential wolverine denning area (PWDA) was thresholded
26 from a 36-year (1985 – 2020) snow reanalysis model with three different spatial discretizations: 1) 480 m grid cells
27 (D480), 2) 90 m grid cells (D90), and 3) 480 m grid cells with implicit representations of subgrid snow spatial
28 heterogeneity (S480). Relative to the D480 and S480 discretizations, D90 resolved shallower snow deposits on
29 slopes between 3050 and 3350 m elevation, decreasing PWDA by 10%, on average. In years with warmer and/or
30 drier winters, S480 discretizations with subgrid representations of snow heterogeneity increased PWDA, even within
31 grid cells where mean 15 May SWE was less than the SWE threshold. These simulations increased PWDA by
32 upwards of 30% in low snow years, as compared to the D480 and D90 simulations without subgrid snow
33 heterogeneity. Despite PWDA sensitivity to different snow spatial discretizations, PWDA was controlled more by
34 annual variations in winter precipitation and temperature. However, small changes to the SWE threshold ($\pm$ 0.07 m)
35 and threshold date ($\pm$ 2 weeks) also affected PWDA by as much as 82%. Across these threshold ranges, PWDA was
36 approximately 18% more sensitive to the SWE threshold than the threshold date. However, the sensitivity to the
37 threshold date was larger in years with late spring snowfall, when PWDA depended on whether modeled SWE was
38 thresholded before, during, or after spring snow accumulation. Our results demonstrate that snow thresholds are
39 useful but may not always provide a complete picture of the annual variability in snow-adapted wildlife denning
40 opportunities. Studies thresholding spatiotemporal datasets could be improved by including 1) information about the
41 fidelity of thresholds across multiple spatial discretizations, and 2) uncertainties related to ranges of realistic
42 thresholds.

43 ## 1. Introduction

44 Generalizing environmental data using thresholds can present information in a way that is more easily understood,
45 communicated, and applied for decision-making purposes. Conceptually, thresholds are static constraints intended to
46 partition the areas, timing, and/or prevalence of data greater or less than some scientifically or managerially relevant
47 limit. In the field of snow science, thresholds are used to classify snow cover and snow absence from remotely-
48 sensed observations (Dozier, 1989; Hall and Riggs, 2007; Sankey et al., 2015), partition snow accumulation and
49 snowmelt seasons (Cayan, 1996; Hamlet et al., 2005; Mote et al., 2005; Serreze et al., 1999), and parameterize

50 modeled processes like snow-layer formation and merging (e.g., Clark et al., 2015; Liston and Elder, 2006;
51 Wigmosta et al., 2002), rain and snow precipitation partitions (Auer, 1974; Harder and Pomeroy, 2013), and snow
52 holding capacity on steep slopes (Bernhardt and Schulz, 2010). Thresholds are also used to identify drought
53 conditions in snow-dominated watersheds (Dierauer et al., 2019; Harpold et al., 2017; Heldmyer et al., 2023) , and
54 the associated "decision trigger" and "tipping point" thresholds that determine water use and allocation in regulated
55 basins (Herman and Giuliani, 2018; Kwadijk et al., 2010; Shih and ReVelle, 1995). However, despite widespread
56 use, thresholds are often developed for specific applications, and over short time intervals, decreasing the likelihood
57 that a threshold developed for one purpose could be applied in an identical manner to different periods of time, or to
58 environmental products with different characteristics (Härer et al., 2018; Jennings et al., 2018; Maher et al., 2012;
59 Pflug et al., 2019).

60 Here, we focus on snow thresholds that have been used increasingly over the past decade to identify regions with
61 conditions suitable for the survival of snow-adapted wildlife. Many studies use thresholds that focus on snow
62 characteristics like snow depth, snow cover, snow density, snow water equivalent (SWE), and snowmelt season
63 snow persistence, which can be important for denning, migration, and food-availability for species like wolverines
64 (*Gulo gulo*), polar bears (*Ursus maritimus*), and Dall sheep (*Ovis dalli dalli*) (Barsugli et al., 2020; Durner et al.,
65 2013; Liston et al., 2016; Mahoney et al., 2018; McKelvey et al., 2011; Sivy et al., 2018). However, relatively few
66 studies simulate snow at spatial resolutions that correspond to the features that drive snow habitat (e.g., Glass et al.,
67 2021; Liston et al., 2016; Mahoney et al., 2018). For instance, wolverines rely on snow drifts for maternal and natal
68 denning. These drifts often form alee of obstructions near the forest edge and in talus fields (e.g., Fig. 1, star). Yet,
69 few models simulate snow at den-scale spatial-resolutions (< 10 m), and represent the physical processes that
70 control the formation of dens, like wind-redistribution, preferential deposition, avalanching, and microtopographic
71 shading. This is particularly the case for species status assessments which often attempt to quantify wildlife habitat
72 at large regional extents where high-resolution snow simulations with complex physical processes would be
73 computationally prohibitive. Thresholds are therefore used to facilitate the relationship between a coarser-resolution
74 representation of snow, and the finer-scale feasibility of wildlife habitat. The validity of this approach is debated
75 (e.g., Araújo and Peterson, 2012; Barsugli et al., 2020; Boelman et al., 2019; Bokhorst et al., 2016; Copeland et al.,
76 2010; Magoun et al., 2017). For example, coarser-scale representations of snow may resolve the larger-scale
77 meteorological influences on habitat availability, but coarser-scale representations of snow likely overlook the
78 smaller-scale refugia that could continue to support habitat, even with future changes to climate.

79 This study builds on work from Barsugli et al. (2020), who used physically-based simulations to identify regions
80 that could support wolverine denning using a SWE threshold (0.20 m) on a static date (15 May) corresponding to the
81 tail end of the maternal denning period(Copeland et al., 2010; McKelvey et al., 2011; USFWS, 2018). This 0.20 m
82 SWE threshold was chosen based on 15 May SWE that corresponded to known wolverine denning sites from a 250
83 m snow simulation (Barsugli et al., 2020; Ray et al., 2017; USFWS, 2018). Barsugli et al. (2020) found that, relative
84 to previous studies that used ~10 km products (Laliberte and Ripple, 2004; McKelvey et al., 2011), snow
85 simulations at 250 m resolution were able to better resolve SWE persistence, and increased habitat, on shaded north-
86 facing slopes. 250 m simulations also increased the overall prevalence of snow that could support wolverine dens,
87 both in current and future climates, over Colorado and Montana Rocky Mountain domains.

88 Here, we extend the findings from Barsugli et al. (2020), testing the difference in wolverine denning support defined
89 using thresholds (0.20 m SWE on 15 May) and a historic snow reanalysis with different spatial discretizations (Fig.
90 1). These discretizations include: 1) discrete 480 m grid cells (D480), 2) discrete 90 m grid cells (D90), and 3) 480
91 m grid cells with implicit representations of subgrid SWE spatial heterogeneity (S480). These discretizations
92 straddle the 250 m resolution used by Barsugli et al. (2020) and include both discrete (D480 and D90) and implicit
93 (S480) representations of snow distribution. These reanalyses, which combine snow modeling and remotely-sensed
94 observations of snow cover (more in Sect. 2.2), also resolve snow volume and distribution in mountain terrain
95 significantly better than more common modeling approaches (Pflug et al., 2022; Yang et al., 2021). We focus on the
96 same Colorado Rocky Mountain domain used by Barsugli et al. (2020) over a longer period of 36 years, spanning
97 1985 to 2020. We address the following research questions: **1) how does the spatial discretization of snow**
98 **influence estimates of potential wolverine denning area (PWDA)? and 2) is the sensitivity of PWDA to**
99 **different snow spatial discretizations greater or smaller than the sensitivity to annual changes in winter**
100 **climatic conditions?** We also identify the spatial locations and causes of the greatest differences PWDA, and
101 evaluate sensitivities to small uncertainties in both SWE thresholds ($\pm$ 0.07 m) and threshold dates ($\pm$ 2 weeks).
102 More generally, this study highlights shortcomings, opportunities, and tradeoffs to thresholding spatial snow
103 products, and serves as a roadmap for future wildlife habitat assessments.
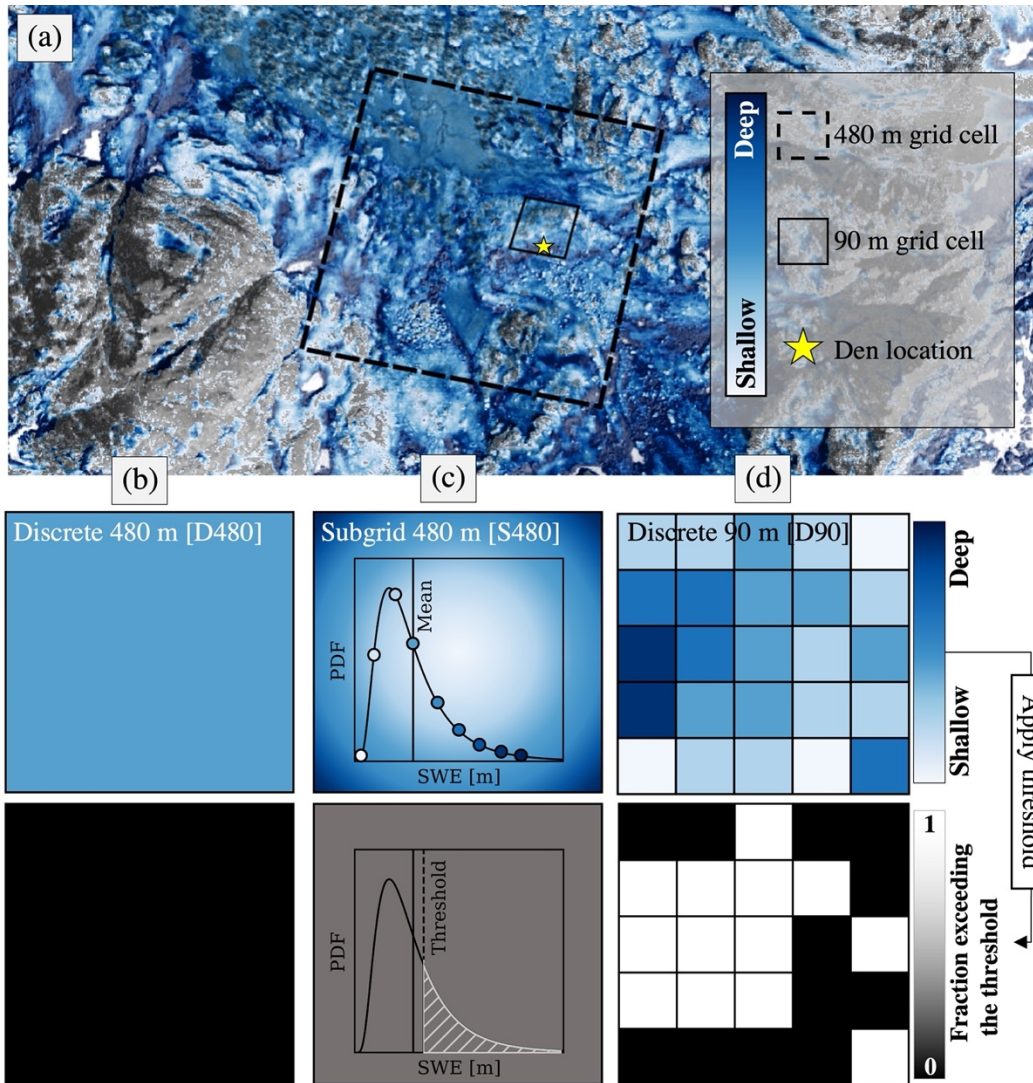
104

105 Figure 1. SWE spatial heterogeneity inferred from airborne lidar at 1 m resolution, compared to 480 and 90 m grid
106 cells, and a point (star) with a snow drift suitably deep for wolverine denning (a). SWE is simulated in this study
107 using three different spatial discretizations: 480 m discrete grid cells (D480, column b), 480 m grid cells with
108 subgrid SWE heterogeneity (S480, column c), and 90 m discrete grid cells (D90, column d). The fraction of the area
109 that could support wolverine denning is estimated for each discretization using a 0.20 m SWE threshold on 15 May.
110 The fraction of the area exceeding the SWE threshold is binary (fully greater than or less than the threshold) for
111 discrete grid cells (b and d), while the area exceeding the SWE threshold for the S480 discretization (c) is defined by
112 the fraction of the grid cell SWE distribution exceeding the threshold (white hatching)

113 **2. Domain and Data**

114 **2.1. Domain**

115 We focused this work over Rocky Mountain National Park in Colorado state (Fig. 2). This domain is home to
116 several snow-adapted wildlife species, and has been included in wolverine habitat assessments (Barsugli et al., 2020;
117 McKelvey et al., 2011; USFWS, 2018). Barsugli et al. (2020) estimated most of the terrain supportive of wolverine
118 habitat in this region to be between 2700 and 3600 m of elevation. Although this area does not currently support a
119 reproductive population of wolverines, this region is of potential interest for wolverine reintroduction. More
120 information about wolverine habitat can be found in the U.S. Fish and Wildlife Service species status assessment
121 (USFWS, 2018).

122   The Rocky Mountain National Park domain contained several snow observations (Fig. 2). These observations
123   include 28 snow telemetry (SNOTEL) stations, deployed and managed by the National Resources and Conservation
124   Service. These stations use snow pillows to measure the weight of snowpack and resulting SWE. A distributed lidar
125   observation of snow depth in southernmost portion of the domain was also collected by the National Center for
126   Airborne Laser Mapping in May 2010. These observations were used to assess the accuracy of the SWE reanalysis
127   discussed in Sect. 2.2.

2.2. SWE Reanalyses

129   SWE was calculated over the Rocky Mountain domain (Figure 2) from a popular satellite-era (water years 1985 –
130   2020) probabilistic snow reanalysis (Margulis et al., 2019, 2016, 2015) performed at 3 arcseconds (~90 m) and 16
131   arcseconds (~480 m). This reanalysis was generated at each individual grid cell using an ensemble of simulations
132   forced by the Modern-Era Retrospective analysis for Research and Applications, Version 2 (MERRA-2; Gelaro et
133   al., 2017), and simulated using the simplified Simple Biosphere Model, Version 3 (Xue et al., 1991) coupled with
134   the Liston (2004) snow depletion curve. The forcing dataset was downscaled to the simulation grid (Girotto et al.,
135   2014; Margulis et al., 2015) before running the land surface model. Model ensemble members were provided
136   different 1) precipitation multipliers (influencing total snow mass), 2) snow albedo decay functions (influencing the
137   rate of snow ablation), and 3) parameterizations of subgrid snow spatial variability (influencing subgrid snow cover
138   during snowmelt), among other parameters. The reanalysis then reweighted the ensemble members to most-heavily
139   favor those that matched the snowmelt season evolution of fractional snow covered area from 30 m Landsat
140   observations. We expect uncertainties and errors in the snow reanalysis owing to both errors in meteorological
141   forcing data (e.g., Daloz et al., 2020; Liu and Margulis, 2019) and errors with the snow model (e.g., Feng et al.,
142   2008; Xiao et al., 2021)However, the ensemble approach used by this reanalysis adjusted modeled snow
143   accumulation and depletion to track remote sensing observations of snow cover depletion, which has shown the
144   capability to bias-correct SWE and implicitly account for difficult-to-simulate processes like precipitation lapse
145   rates, wind-loading/scour, avalanching, and forest-snow processes (e.g., Pflug et al., 2022; Yang et al., 2021).

146   Relative to SNOTEL observations, which are not used by the snow reanalysis, the reanalysis exhibited a SWE
147   coefficient of correlation of 0.82 between 1985 and 2020 in the Rocky Mountain domain (Fig. S1). On average, the
148   reanalysis was biased low relative to the snow pillow observations by approximately 23%. However, this could be
149   attributed to the location of SNOTEL observations in forested clearings (Fig. 2a) which typically have SWE deeper
150   than the terrain covered by the 480 and 90 m pixels(e.g., Livneh et al., 2014; Pflug et al., 2022).While the snow
151   reanalysis used in this study is ultimately a model product and subject to a number of modeling uncertainties, the
152   SWE simulated by the 90 m and 480 m discretizations agreed closely with each other and with ground observations.
153   Therefore, spatial differences in 15 May SWE, and the resulting distribution of snow that exceeded the SWE
154   threshold (e.g., Fig. 1) was attributable to differences in the interactions between the static SWE threshold and
155   different spatial discretizations of snow.

156   For the 480 m grid cells with subgrid snow variability (Fig. 1c, S480), the heterogeneity of SWE was estimated
157   using a method developed by Liston (2004). This method assumes that the subgrid heterogeneity of SWE
158   accumulation is lognormally distributed, and is dictated by a time-constant coefficient of variation (CoV),

159
$$CoV = \frac{\sigma}{\mu},$$

160   (1)

161   where μ is the grid cell mean SWE and σ is the standard deviation of the SWE within that grid cell. The CoV of
162   subgrid SWE accumulation (Fig. 2b and 2c) was determined for each 480 m grid cell using the most common
163   pattern of SWE accumulation from the overlapping 90 m reanalysis grid cells (Fig. 1d) between 1985 and 2020
164   (detailed further in Text S1). In Sect. 3.1, we discuss how CoV was used to estimate the temporal evolution of
165   subgrid SWE heterogeneity.

166
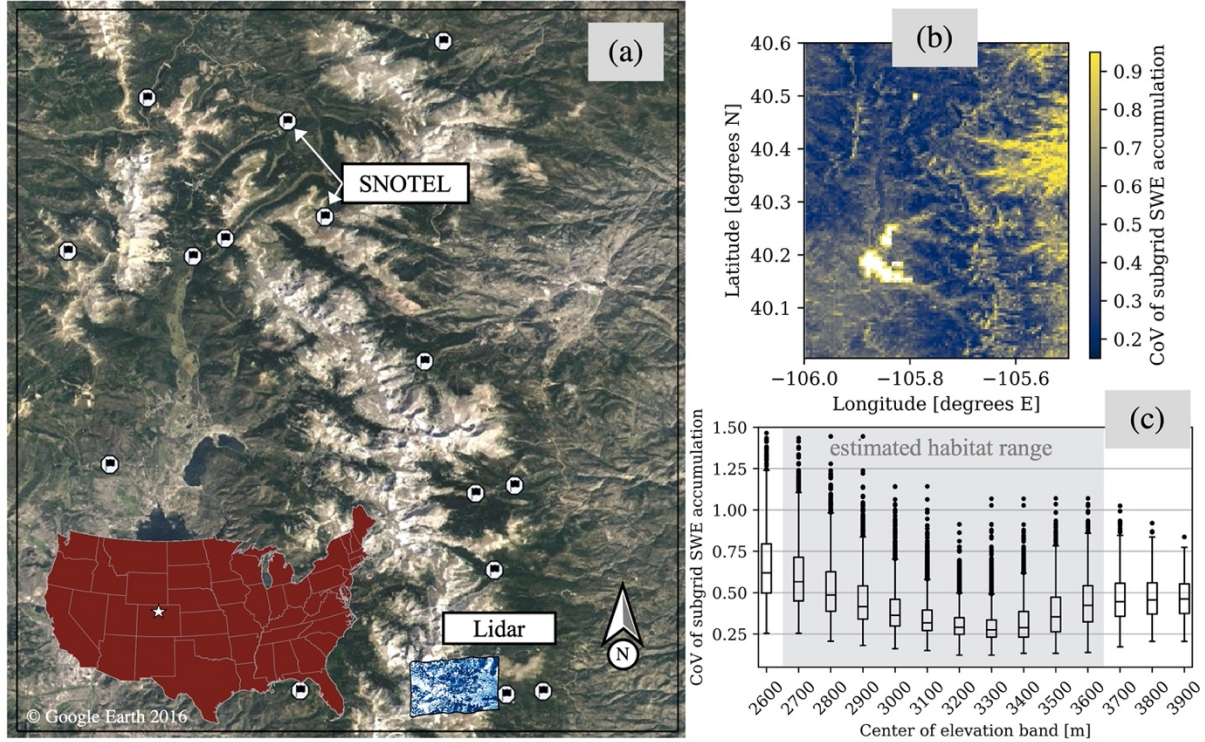
168 Figure 2. Rocky Mountain National Park study domain. The location of SNOTEL observations and lidar snow depth
169 observations are superimposed in the terrain map (a). The 480 m coefficient of variation of subgrid SWE
170 accumulation is shown both spatially (b) and across 100 m elevation bands (c).

3. Methods

172 The methods evaluate the impacts of snow spatial discretizations and winter climatic conditions on assessments of
173 total area suitable for denning wolverines. We investigated three different spatial discretizations; two discretizations
174 using more common discrete representations of snow, and one with an implicit representation of subgrid snow
175 heterogeneity (see Sect. 3.1). For each, potential wolverine denning area (PWDA) was calculated using a static
176 SWE threshold (0.20 m) on a static spring date (15 May) (Sect. 3.2). Finally, we partitioned years with winter
177 precipitation magnitude and precipitation phase climate categories (wet, dry, cold, and warm) (see Sect. 3.3). These
178 categories were used to examine whether winter climatic conditions or model representations of snow spatial
179 distribution most-influenced estimates of PWDA.

3.1. Subgrid SWE evolution

181 The temporal evolution of subgrid SWE heterogeneity was estimated for 480 m grid cells (Fig. 1, S480) using
182 methods developed by Liston (2004) (Fig. 3). Provided the reanalysis grid cell mean SWE (μ) from a D480grid cell
183 (Fig. 1b), and a CoV of subgrid SWE accumulation (Fig. 2b), the probability distribution of subgrid SWE for that
184 grid cell ($f(SWE)$) was calculated using a lognormal distribution,

185

186
$$f(SWE) = \left(\frac{1}{SWE\zeta\sqrt{2\pi}}\right) exp\left[-\frac{1}{2}\left[\frac{\ln(SWE) - \lambda}{\zeta}\right]^2\right],$$

187
(2)

188
$$\lambda = \ln(\mu) - \frac{1}{2}\zeta^2,$$

189
(3)

$$\zeta^2 = \ln(1 + CoV^2).$$

$$(4)$$

Figure 3b demonstrates the subgrid distribution of SWE in two winter periods (t_a^1 and t_a^2) assuming the mean SWE evolution from Fig. 3a, a CoV of 0.50, and Eq. 2 – 4.

In the snowmelt season, the Liston (2004) methodology assumes spatially-uniform snowmelt, causing snow disappearance first in locations with thinner SWE, and last in locations with deeper SWE. This can be conceptualized as taking the subgrid distribution of snow at peak SWE (Fig. 3b, t_2^a), and adjusting it downwards by a constant amount to reflect spatially-uniform melt (SWE_m) (Fig. 3c). In doing so, snow only exists for portions of the gridcell where $f(SWE)$ at peak SWE was greater than SWE_m. Therefore, the fractional snow-covered area (fSCA) of the grid cell could be calculated from the fraction of the distribution ($f(SWE)$) with SWE greater than SWE_m,

$$fSCA = \int_{SWE_m}^{\infty} f(SWE)dSWE.$$

$$(5)$$

Since SWE_m can exceed the amount of SWE that exists in some locations at peak SWE timing, and since SWE cannot be less than 0 m (snow-absent), the change in gridcell mean SWE (μ) throughout snowmelt will not necessarily equal SWE_m. Rather, μ throughout the snowmelt season can be calculated from the expected value of the melt-shifted distribution (Fig. 3c),

$$\mu = \int_{SWE_m}^{\infty} [SWE - SWE_m]f(SWE)dSWE.$$

$$(6)$$

In this study, we were provided μ from the reanalysis at each 480 m grid cell and daily timestep. Using the CoV calculated from the overlapping D90 data (Fig. 2b), and maximum annual μ at each grid cell, we calculated the SWE distribution (Eq. 2) for each grid cell at peak SWE timing. Then, using a Newton-Raphson solver, we solved the SWE_m for each grid cell that caused μ from Eq. 6 to match D480 μ at each grid cell on 15 May.

The Liston (2004) subgrid SWE parameterization discussed above operates under several assumptions. Like many other studies (e.g., Donald et al., 1995; Helbig et al., 2021; Jonas et al., 2009), Eq. 2 assumes that the distribution of snow accumulation at scales finer than the grid cell resolution can be represented by a lognormal distribution. We tested this assumption by evaluating the distribution of 1 m lidar snow depth observations (Fig. 2a) that fell within 480 m grid cells. The Kolmogorov-Smirnov (KS) statistic, or maximum difference between cumulative distribution functions, was used to test how well different theoretical distributions (e.g., normal, lognormal, gamma, Rayleigh, chi, etc.) used by a variety of snow studies (e.g., He et al., 2019; Helbig et al., 2015; Mendoza et al., 2020; Pflug and Lundquist, 2020; Skaugen and Melvold, 2019) matched the lidar-observed snow depth distributions. The KS statistic for the lognormal distribution (Eq. 2) was 0.12 ± 0.05, and was significantly worse (greater than 0.22) when comparing the observed lidar distributions versus other common distributions, like normal and gamma distributions. While not perfect, these results showed that subgrid snow heterogeneity was approximated best by lognormal distributions. The Liston (2004) subgrid methodology also assumed that the CoV of subgrid SWE accumulation was constant, resulting in a linear increase in SWE variability (standard deviation) with mean SWE throughout the snow accumulation season (Fig. 3b). While we lacked validation data to test this, this assumption is the basis for other modeling approaches, which scale snow input using information from historic snow accumulation patterns (Liston, 2004; Luce et al., 1998; Pflug et al., 2021; Vögeli et al., 2016). Finally, although subgrid snowmelt is not spatially-uniform, melt-season snow heterogeneity is often modeled well by assuming uniform snowmelt. This is due to the outsized influence of snow accumulation spatial heterogeneity on snowmelt onset timing and snowmelt rates (Egli et al., 2012; Luce et al., 1998; Lundquist and Dettinger, 2005; Pflug and Lundquist, 2020). Here, we acknowledge that this approach operates on multiple assumptions (discussed above), all of which could vary in accuracy on grid cell level. However, this approach may also provide the opportunity to implicitly represent the heterogeneity of snow in complex terrain and the fraction of the area that could be more supportive for denning habitat (e.g., Fig. 1). We discuss this more in Section 3.2. Readers should refer to Liston (2004) for more information about the subgrid snow methodology described in this section.
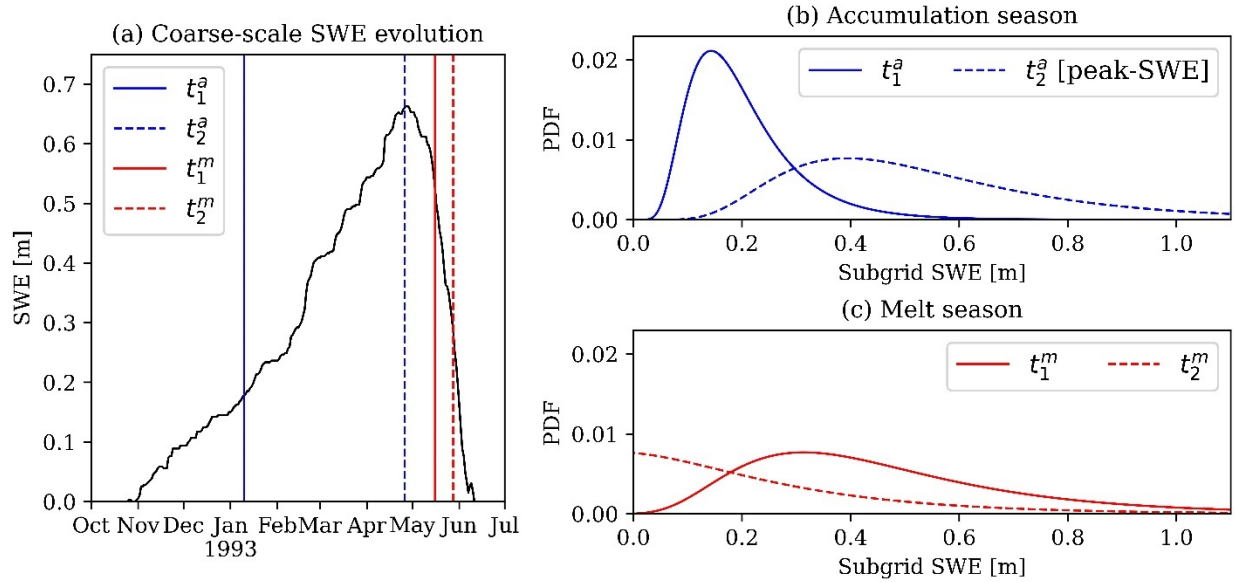
Figure 3. An example of the Liston (2004) subgrid SWE parameterization assuming CoV = 0.5, and SWE evolution for a 480 m grid cell in a random year (panel a). Subgrid SWE distributions are shown for two times (*t,* subscripts 1 and 2) in the accumulation (superscript a) and melt (superscript m) seasons (panels b and c, respectively). The timing of each date corresponds to the matching vertical bar in panel a.

3.2. Thresholding wolverine habitable area

The area that could support denning wolverines was calculated for each of the discretizations in each year using a SWE threshold of 0.20 m on 15 May, in accordance with previous studies (e.g., Barsugli et al., 2020; Copeland et al., 2010; McKelvey et al., 2011). For the D480 and D90 discretizations, each cell's denning fraction (DF) was classified as fully-suitable for denning (DF = 1.0) or unsuitable (DF = 0.0) if the 15 May grid cell SWE was greater than or less than 0.20 m, respectively. For the S480 discretization, DF was calculated for each grid cell using:

$$DF = \int_{SWE_m+\beta}^{\infty} f(SWE) dSWE,$$

(5<s>7</s>)

which represented the portion of the cell's SWE distribution greater than the SWE threshold ($\beta = 0.20$ m). PWDA was calculated for each discretization as the sum of DF (in space), multiplied by grid cell area.

Relative to DF calculated from a discrete 480 m grid cell (D480), DF calculated over the same area from the finer-scale discretizations (S480 and D90) could have one of four possible relationships. First, the mean SWE of the D480 grid cell, and the finer-scale distribution of SWE (S480 and D90), could both be entirely greater than the 0.20 SWE threshold. This results in a fully-suitable denning fraction (DF = 1.0) for all discretizations (Fig. 4a). DF would also agree in regions where all discretizations have SWE below 0.20 m (Fig. 4d), resulting in no denning opportunities (DF = 0.0). The scenarios shown in Fig. 4b and Fig. 4c are where DF is sensitive to the discretization. Figure 4b shows a scenario where the coarse-scale mean SWE is sufficiently deep enough to be classified as fully-suitable for denning (SWE > 0.20 m), even though some portion of that grid cell contains SWE that is shallower than the SWE threshold. Therefore, using a finer-scale discretization would result in a net loss in DF, the magnitude of which is shown by the red hatching in Fig. 4b. The opposite could be true for instances where coarse-scale mean SWE falls below the 0.20 m SWE threshold, thereby underestimating denning opportunities relative to finer-scale representations that resolve some deeper snow deposits (Fig. 4c, blue hatching). Here, the three reanalysis discretizations (D480, D90, and S480) were provided identical meteorological forcing, and when coarsened to 480m resolution, had SWE that agreed to within 1%, on average on 15 May. Therefore, the degree to which the scenarios shown in Fig. 4b and 4c occur were the drivers of differences to wolverine denning opportunities.
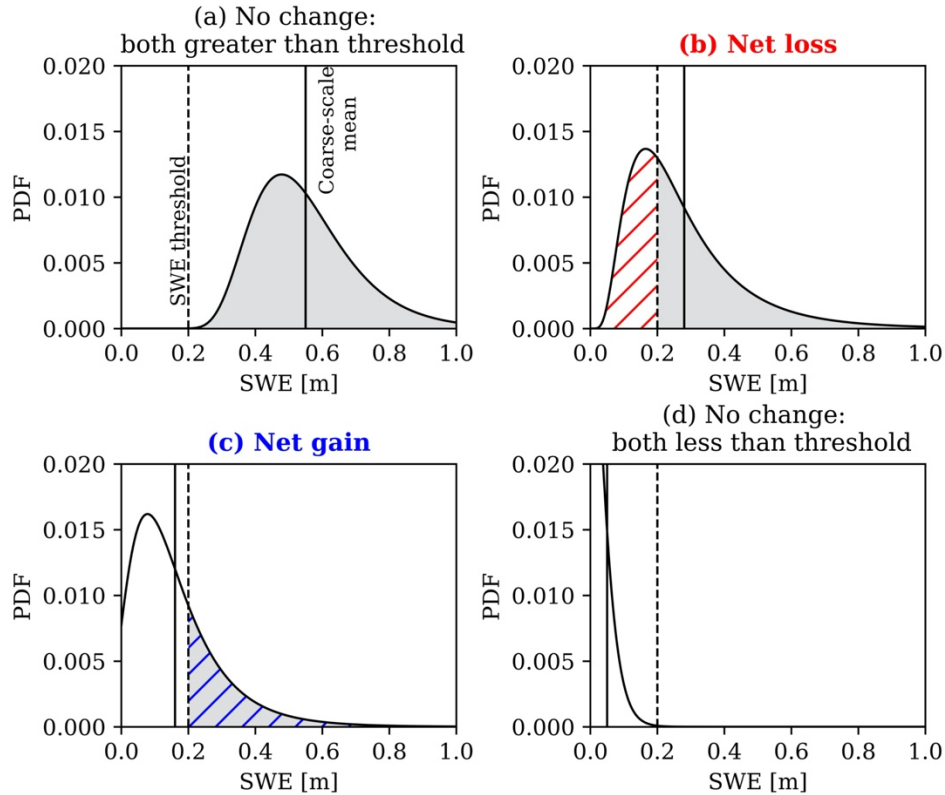
Figure 4. Conceptual portrayal of the similarities (a and d) and differences (b and c) in DF for a 480 m discrete grid cell (vertical solid line) and a finer-scale representation (distribution) of SWE over the same area. The vertical dashed lines represent the 0.20 m SWE threshold. Shaded areas show the portion of the distribution with SWE greater than the threshold. Hatched areas demonstrate differences in DF between the coarser and finer-scale discretizations of SWE.

3.3. Categorizing winter climate categories

To determine PWDA sensitivity to different climatic conditions, we identified years from the reanalysis with different winter precipitation magnitude and phase (rain versus snow). Here, winter is defined by periods between October 1st and the date of domain peak SWE volume. Following work from Heldmyer et al. (2023), we used domain average cumulative winter precipitation and the fraction of the winter precipitation that fell as snow (both from the reanalysis) as indices for winter precipitation magnitude and the temperature at which precipitation fell. Using a percentile, we separated years that fell at least that far from the 1985 – 2020 median precipitation magnitude and fraction of snow precipitation. In doing so, we partitioned years with wet, dry, cold, and warm winter climate categories. We did this separation using a range of percentiles until the statistical difference (measured using the Mann-Whitney u-test) in D480 PWDA was maximized between the years with different climatic conditions (warm, cold, wet, dry, and typical). To avoid spurious results, this percentile was also adjusted to ensure that each climate category included at least 6 years. This approach maximized the difference in interannual PWDA as a function of different winter climatic conditions. This was then used as the baseline to compare how much more or less sensitive PWDA was to the different SWE spatial discretizations.

4. Results

Over low-elevation forested grid cells (< 2800 m), SWE accumulation variability was large relative to the smaller amounts of snow, resulting in large CoV (typically between 0.50 and 0.80) (Fig. 2b and 2c). On mid-elevation slopes (2800 – 3300 m), CoV tended to be smaller (approximately 0.30, on average). However, CoV increased again at higher elevations (> 3300 m), and particularly on the leeward side of peaks. This was expected given the more extreme terrain and increased spatial variability of snow from wind-drifting, preferential deposition, cornice formation, and avalanching.

294 The difference in PWDA was maximized between 1) warm and cold years, and 2) wet and dry years, that had winter
295 precipitation magnitude (Fig. 5a, x-axis) and precipitation phase (Fig. 5a, y-axis) that fell above the 77th and below
296 the 23rd percentiles ($\pm$27th percentile from the median). These climate conditions had impacts on the evolution of
297 SWE and snow-covered area (Fig. 5b and Fig. 5c). On average, as compared to years with normal winter
298 precipitation magnitude and phase (Fig. 5a, white region), cold years and wet years had peak SWE volume that was
299 23% and 28% greater, respectively. This was opposed to warm years and dry years, with peak SWE volume that was
300 21% and 31% smaller, on average, than typical water years. The timing of peak-SWE was driven most by the
301 magnitude of winter precipitation. In fact, average peak-SWE timing was 28 days later for wet years than dry years.
302 Snow disappearance timing (snow-covered area $< 200\ km^2$) was also 21 days later for wet years than dry years.
303 Statistically, the timing of snow disappearance, crucial for wolverine denning habitat, was explained well by the
304 peak-SWE volume (r = 0.82) and the date of peak-SWE (r = 0.63), both of which were influenced more by winter
305 precipitation magnitude than temperature.
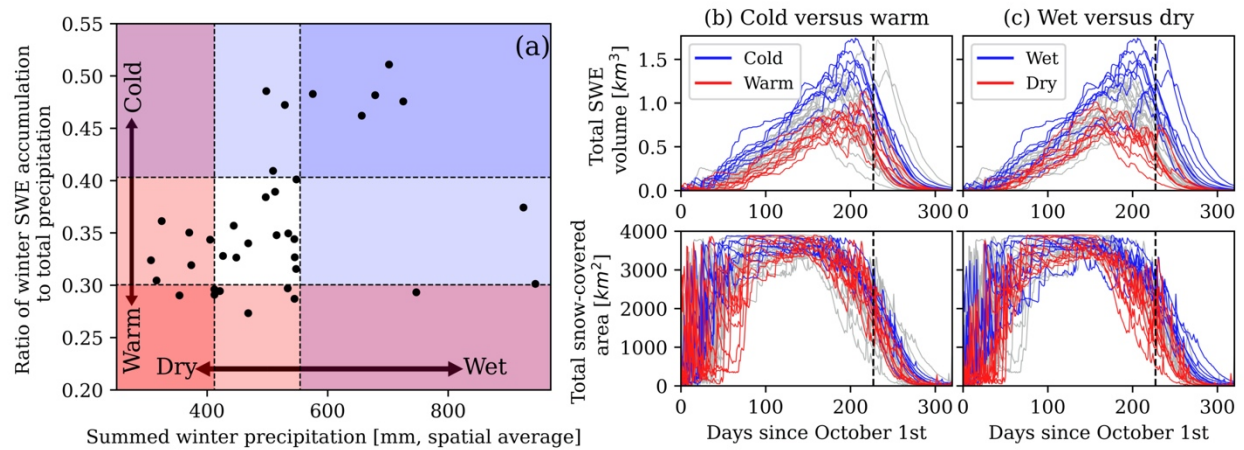
306

307 Figure 5. Annual climatic conditions grouped into categories based on winter precipitation magnitude (a, horizontal-
308 axis) and precipitation phase (a, vertical-axis) outside the 23rd and 77th percentiles (a, dashed lines). The evolution of
309 SWE volume and snow cover are compared for warm versus cold (column b) and wet versus dry years (column c).
310 Vertical dashed lines in columns c and d indicate 15 May.

311 In all years except dry 2002, PWDA was smaller for the D90 discretization than the D480 discretization (Fig. 6).
312 This resulted in a 10% reduction to the 36-year median PWDA (Fig. 6b). The PWDA differences between the D480
313 and S480 discretizations varied more on an annual basis. For years with D480 PWDA less than $1000\ km^2$, S480
314 discretizations increased PWDA by up to 30%, 11% on average. However, in years with PWDA greater than
315 $1000\ km^2$, S480 PWDA was approximately 3% smaller, on average, than D480 PWDA. In short, the S480
316 discretization tended to have smaller annual swings in PWDA than the D480 discretization. The causes of these
317 PWDA disagreements are discussed in Sect. 5.1. Despite the annual differences in D480 and S480 PWDA, the 36-
318 year median PWDA for these discretizations agreed to within 1% (Fig. 6b).
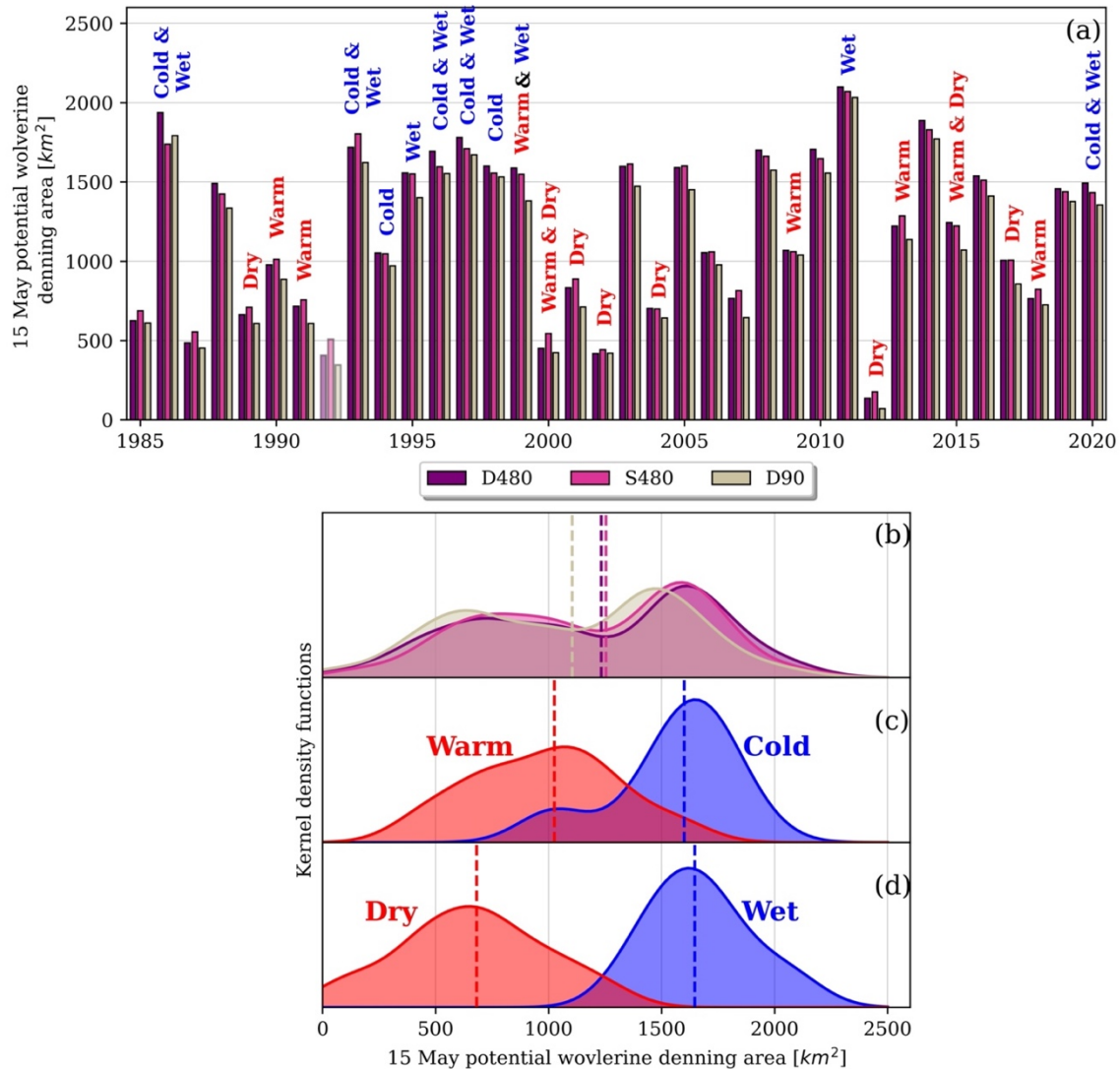
Figure 6. 15 May PWDA compared annually for three different spatial discretizations (a). Lower panels show the kernel distributions for the data in panel a, separated based on the spatial discretization (b), temperature categories (c), and precipitation categories (d). The medians of each distribution are shown by the vertical dashed lines (b – d). The data in panels c and d include data from all three spatial discretizations. The data from WY1992 (a, faded bars) exhibited artifacts, and was excluded from the kernel distributions (b-d).

Even though PWDA was sensitive to different spatial discretizations (Fig. 6b), PWDA across the 36-year period was not statistically different between any of the three discretizations (p > 0.48). Conversely, the difference in 15 May PWDA was significantly larger between the years with different winter climate categories (Fig. 6c and 6d).Differences in PWDA between years with warm and cold conditions were statistically significant (p = 1×10^{-5}). Given that 15 May snow covered area were similar between warm and cold years (Fig. 5b), this difference between warm and cold years in Fig. 6c show that changes to PWDA were driven by changes to SWE magnitude and the area with SWE exceeding the SWE threshold. Dry and wet years exhibited larger differences to both 15 May SWE and snow cover (Fig. 5c), resulting in PWDA (Fig. 6d) that was even more different between the years with these climate conditions (p = 1×10^{-8}). The impact of these warm, dry, cold, and wet climate conditions resulted in the bimodal distributions in PWDA shown for the different discretizations across the full time period (Fig. 6a). While PWDA was not statistically different between cold and wet years (p = 0.34), the distribution of PWDA in dry years was significantly smaller than the distribution of PWDA in warm years (p = 0.001), showing that PWDA was more sensitive to conditions that reduced snow habitat, like warm and dry conditions.

338 The results from Fig. 6 suggested that changes in PWDA across annual periods of differing climatic conditions, or
339 across future periods with expected changes in climate (e.g., Barsugli et al., 2020) should be informative from a
340 species status assessment perspective, regardless of the snow spatial discretizations that we tested here. However, as
341 noted above, the S480 discretization increased PWDA by 11% on average in low snow years, with increases as large
342 as 30% for individual years. These low snow years often corresponded with drier and/or warmer winter conditions,
343 the latter of which are expected in the future. For example, the average air temperature during December, January,
344 and February precipitation events during warm years in the reanalysis record was approximately 0.8° higher than
345 winter precipitation events in typical years. These conditions are consistent with what is projected for this region by
346 2055 (Eyring et al., 2016; Scott et al., 2016). This suggests that the disparity between habitat inferred from discrete
347 grid cells, and grid cells with subgrid snow heterogeneity, could be of greater importance for future snow habitat
348 assessments. Additionally, using PWDA as the sole metric for evaluating differences in annual opportunities for
349 wolverine denning may oversimplify the degree to which static thresholds and different spatial discretizations
350 interact. For instance, PWDA inferred on a static date (15 May) compares very different regimes of the snow season
351 as wet years had peak SWE timing, and snowmelt season onset, that was 21 days later than typical snow seasons
352 (Fig. 5). Since shallower snow melts more readily than deeper snow (provided the same energy), comparing SWE
353 on a static date in years with very different conditions neglects the different rates of habitat depletion for a few days
354 on either side of the date threshold. These issues are investigated more in Sect. 5.

5. Discussion

356 In this section we diagnose the causes for disagreements in the frequency and locations at which 15 May SWE
357 exceeded the 0.20m SWE threshold between the three spatial discretizations of snow (Sect. 5.1). We also investigate
358 how the use of a static SWE threshold and threshold date, may obscure the picture of interannual changes to
359 wolverine denning habitat availability (Sect. 5.2). Using these findings, we discuss how information provided from
360 multiple spatial discretizations could provide information about the fidelity and uncertainty of thresholds, as well as
361 the interactions and tradeoffs between spatial discretizations and thresholds, both in context for assessing snow-
362 adapted wildlife habitat, and more broadly for other environmental studies (Sect. 5.3).

5.1. Spatial differences in DF

364 The spatial difference in DF between the three discretizations had annually similar patterns, with the largest
365 differences at locations where the domain had SWE that was near the 0.20 m SWE threshold. This is shown in
366 Fig.7d and Fig. 7e where the spatial DF disagreements that spiked on 15 May 2008 were focused between
367 approximately 2800 and 3200 m of elevation. Relative to the D480 discretization, the S480 discretization tended to
368 increase DF in grid cells at lower elevations where mean SWE was less than the SWE threshold, but some portion of
369 the grid cell had SWE deep enough to exceed the threshold (e.g., Fig. 4c). The opposite effect occurred at higher
370 elevations where mean SWE exceeded the SWE threshold, but the lower-tails of the S480 SWE distributions were
371 below the threshold (e.g., Fig. 4b). As a result, the S480 discretization had a more-gradual increase in thresholded
372 denning availability with elevation, and a downward shift in the elevations that could support denning wolverines
373 (Fig. 7f). In fact, relative to the D480 discretization, the S480 discretization had 23% less interannual variability in
374 the elevation at which equal PWDA existed at higher and lower elevations (Fig. S2a). This was a result of the
375 subgrid representations of SWE heterogeneity which allowed for gradual and fractional ($0.0 \leq DF \leq 1.0$) increases
376 in DF with increases in SWE. This was opposed to the D480 discretization, which could only resolve binary DF (0
377 or 1 for SWE less than and greater than 0.20 m), resulting in larger elevational shifts in the annual locations that
378 could support wolverine denning.
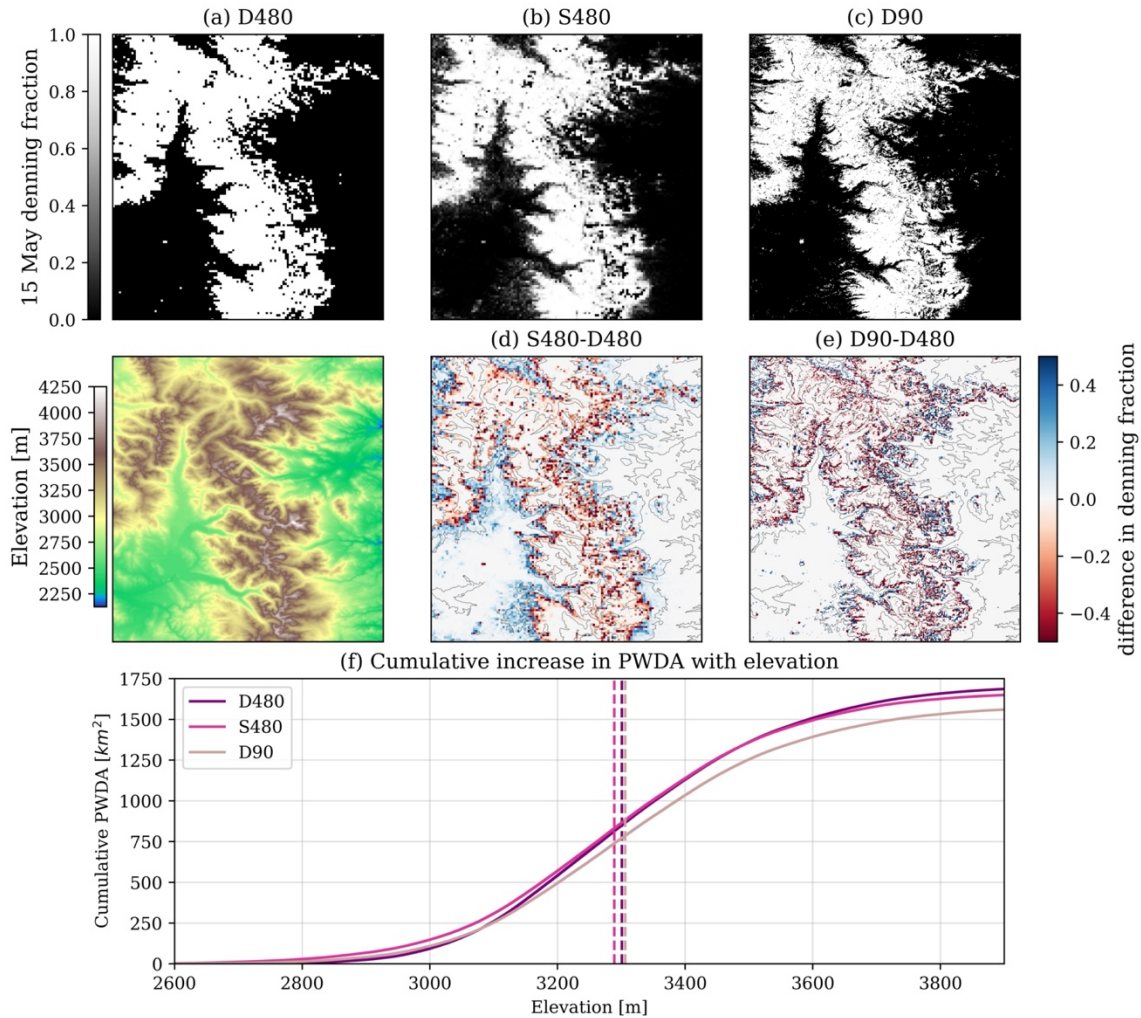
Figure 7. Spatial comparisons of DF for the three discretizations on 15 May 2008. Panel f compares the cumulative PWDA (y-axis) calculated for grid cells sorted in order of increasing elevation (x-axis). Vertical dashed lines show the elevation of median PWDA, or elevation at which PWDA is equal for higher and lower elevations.

Relative to the D480 discretization, the D90 discretization also tended to increase DF at lower elevations. However, all years had reduced D90 DF in elevations higher than approximately 3120m. This was the cause of the 10% reduction in D90 PWDA, relative to the other discretizations (Fig. 6b). These decreases were typically located on unvegetated, exposed, and steep slopes, where it was likely that winter snow retention was decreased, snow sublimation was increased, and sloughing to lower-elevations was more common (Bernhardt and Schulz, 2010; Grünewald et al., 2014; Machguth et al., 2006). This demonstrates the utility of the observation-based reanalysis used in this study, which may have resolved thinner snow deposits on slopes with decreased snow retention and/or enhanced snow removal by processes like sloughing, both of which are among the most-difficult processes to represent with models. The D480 discretization averaged snow from surrounding areas, smoothing out thinner snow deposits resolved by the D90 discretization. Although attempting to resolve subgrid snow heterogeneity, the evolution of SWE assumed by the S480 simulation, which assumed lognormal snow accumulation and spatially-uniform subgrid snowmelt (Fig. 3), may have been less-appropriate for the areas containing these isolated thinner-snow 90 m grid cells. While the D90 discretization decreased total PWDA, D90 snow cover was also patchier (Fig. 7c), which could also influence the movement and connectivity for wolverines (USFWS, 2018) and other snow-adapted species.

Winter precipitation magnitude and temperature influenced the volume of snow and the elevation of the snow line that existed on 15 May in each year. Since the differences in DF between the discretizations were largest at grid cells near the 0.20 m SWE threshold, often located just above the snow line, the spatial pattern of DF differences (e.g.,

Fig. 7) exhibited an interannually-repeatable relationship with the dry, warm, cold, and wet winter climate categories (Fig. 5). To show this, we calculated the differences in DF between all three discretizations (D480 versus S480, D480 versus D90, and S480 versus D90) in all 36 years. Then, for each 480 m grid cell, we identified the climate category that resulted in the greatest mean absolute differences in DF across the three discretizations. The climate categories that had the greatest influence on DF uncertainties covered similar portions of the domain, with 33.7%, 20.9%, 25.2%, and 20.2% being most attributed to dry, warm, cold, and wet conditions, respectively (Fig. 8). At low elevations (2650 – 3050 m), 15 May snow typically existed only in wet years. In those years and elevations, mean SWE for the D480 and D90 discretizations often fell below the 0.20 m SWE threshold. However, the large CoVs of subgrid SWE accumulation in these elevations (Fig. 2) resulted in S480 subgrid SWE distributions with upper-tails that sometimes exceeded 0.20 m (e.g., Fig. 4c) (Fig. 8c). This was in-line with findings from Magoun et al. (2017), who noted suitable denning conditions at lower-elevations, even in instances when the surrounding terrain was predominantly snow-free.

The average differences in DF between the three discretizations were largest in cold years for elevations spanning 3050 – 3150 m, and in warm years for elevations spanning 3150 – 3350 m (Fig. 8). Across this elevation range (3050 – 3350 m), both of the 480 m discretizations (D480 and S480) estimated more denning opportunities than the D90 discretization (Fig. 8c). However, at higher elevations (> 3350 m), DF calculated from the S480 discretization approached DF calculated from the D90 thinner snow deposits (Fig. 8c).
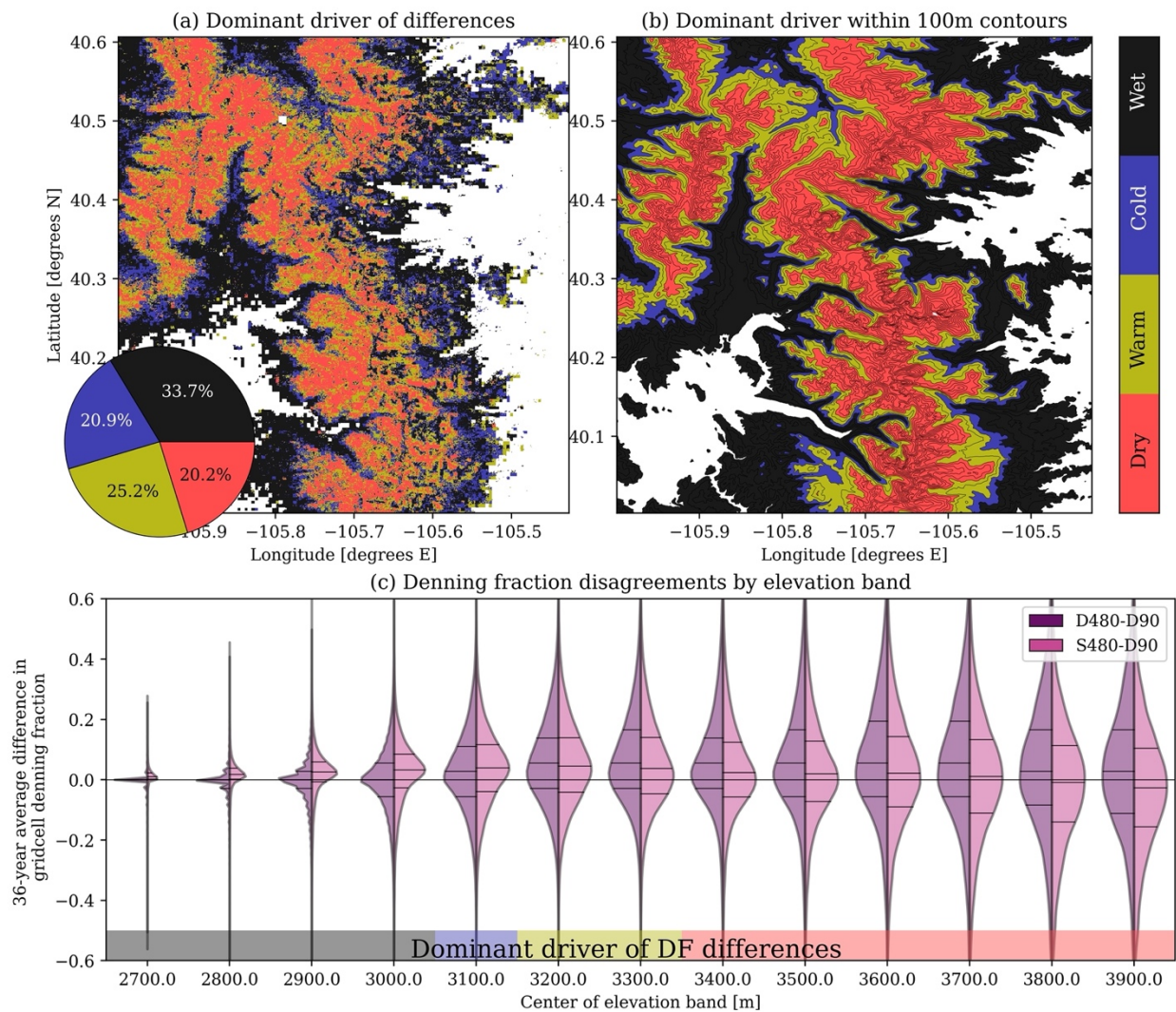
Figure 8. Winter climate categories that most-influenced DF disagreements between the three discretizations (a). Panel b shows the most-prevalent influence from panel a, for 100 m elevation bands. Using DF from the D90

421   discretization as a reference, the 36-year average difference in DF for the D480 and S480 simulations are shown by
422   distributions for each 100 m elevation band (c). Lines inside the distributions show the median and interquartile
423   range.

424   **5.2. Threshold sensitivities**

425   To this point, we assumed confidence in the SWE (0.20 m) and date (15 May) thresholds. However, small changes
426   to either threshold could influence annual estimates of PWDA (e.g., Copeland et al., 2010; Magoun et al., 2017). In
427   Fig. 9, we show PWDA calculated from a range of realistic SWE thresholds and threshold dates. The range of SWE
428   thresholds (0.20 $\pm$ 0.07 m) were determined using a snow depth of 0.50 m, corresponding to observed wolverine
429   dens (USFWS, 2018), and the 90th percentile range of 15 May snow densities from SNOTEL observations (Fig. 2a)
430   between 1985 and 2020 (260 – 540 kg/m^3). The range of threshold dates spanned a period of $\pm$ 2 weeks,
431   corresponding to the difference in peak-SWE timing between dry and wet years (Fig. 5). This month-long time span
432   is also consistent with the observed range of wolverine birth dates (Inman et al., 2012). PWDA sensitivity was
433   calculated using all combinations of SWE and date thresholds, both of which were discretized at 14 equally-spaced
434   increments (Fig. 9, left). Then, the gradients (direction and magnitude of greatest change in PWDA) were calculated
435   from each unique combination of SWE and date thresholds. The gradients were summed using vector addition (Fig.
436   9, right column) to determine 1) the total rate of change in PWDA with changing thresholds (arrow length), and 2)
437   the degree to which PWDA was sensitive to one threshold versus the other (arrow angle). This process was repeated
438   for each discretization and year.
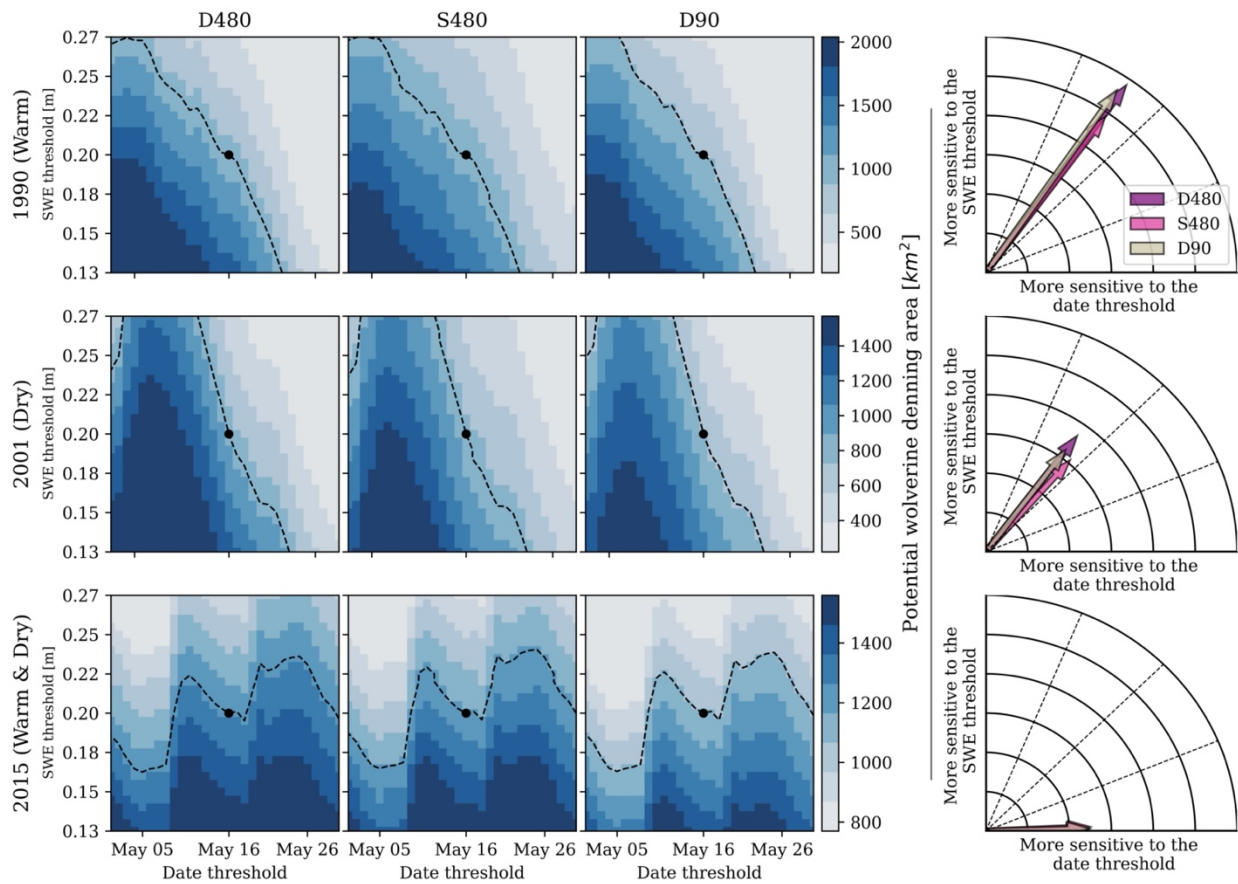
439

440   Figure 9. PWDA calculated using different SWE (y-axes) and date thresholds (x-axes), for the different
441   discretizations (columns), in three different years (rows) with very different sensitivities. PWDA calculated from the
442   default thresholds (0.20 m SWE on 15 May) is shown by the black circle. Combinations of thresholds that could
443   reproduce the default PWDA are approximated by the dashed contour. The rightmost arrows show the total direction
444   and magnitude of PWDA changes with changes in the thresholds.

445 PWDA in warm 1990 was 18% more-sensitive to the SWE thresholds than the threshold dates (Fig. 9, top row). To
446 put this another way, the change in PWDA across a period of $\pm$ 3 days from 15 May was approximately equal to the
447 change in PWDA from adjusting the SWE threshold by $\pm$ 2.5 centimeters. This sensitivity was similar to the
448 average threshold sensitivity from the 36-year reanalysis record (Fig. S2b). However, multiple years exhibited
449 unique sensitivities. For example, spring snowfall between 1 May and 6 May 2001 (Fig. 9, middle row) caused
450 PWDA to both increase and decrease over the range of date thresholds (assuming a constant SWE threshold).
451 Therefore, PWDA changed based on whether the threshold date was before, during, or after the May snowfall event,
452 buffering the degree to which thresholded denning habitat estimates were influenced by the specific winter
453 meteorological conditions that occurred in that year. This effect also occurred in 2015, when 15 May fell between
454 two spring snowfall events (Fig. 9, bottom row). As a result, PWDA tended to increase, on average, over the range
455 of threshold dates, resulting in heightened sensitivities to the date on which denning opportunities were evaluated.
456 These spring snowfall events had large impacts on 15 May PWDA, but are unlikely to accurately represent the
457 habitat opportunities and stresses that wolverine were subject to in that year. This demonstrates the dangers of
458 thresholds applied on static dates, and suggest that metrics over multiple dates (e.g., number of May days exceeding
459 a SWE threshold) and across sequences of years could be more accurate representations of snow refugia.

460 PWDA varied by as much 82% between the realistic thresholds shown in Fig. 9. This was similar in magnitude to
461 the differences in PWDA between years with opposing winter climate anomalies (Fig. 6c and 6d). Across the years
462 evaluated in this study, the sensitivities to the thresholds were largest for the D480 simulation, and smallest for the
463 S480 simulation (Fig. 9 and Fig. S2b). As discussed in Sect. 5.1, the S480 discretization, which represented subgrid
464 snow distribution and fractional changes to DF with changes to the SWE threshold and threshold date, had less
465 sensitivity to annual changes in meteorological conditions. Similarly, small changes in the SWE threshold and
466 threshold date changed the prevalence of snow that exceeded the static threshold for discrete grid cells by larger
467 amounts than the S480 discretization. This suggests that studies with subgrid representations of snow heterogeneity
468 may decrease the overall sensitivity to SWE and date thresholds.

5.3. Threshold caveats and future suggestions

470 The D90 and S480 discretizations provided unique, but different advantages for estimating PWDA. We believe that
471 the upper-elevation decreases in D90 SWE and denning habitat on steep and unvegetated surfaces were realistic.
472 These results were contrary to the findings from Barsugli et al. (2020), who in the same domain, found that finer-
473 scale physically-based simulations resulted in net increases in wolverine denning opportunities. However, this
474 analysis used a joint model and observation-based approach (Sect. 2) that may have implicitly represented decreased
475 snow retention and/or snow sloughing better than the physically based models used by Barsugli et al. (2020). The
476 discretization with subgrid snow heterogeneity (S480), which is not as commonly used, had less-dramatic swings in
477 PWDA with changes in annual winter climatic conditions (Fig. 6) and thresholds (Fig. 9). We therefore think that
478 subgrid representations of snow may be important for habitat assessments, especially given that snow deposits
479 suitable for denning at scales of 10 m or less sometimes occur in regions with otherwise little snow (Magoun et al.,
480 2017).

481 The results of this study suggest that uncertainties provided from combinations of multiple discretizations, applied
482 across a range of realistic thresholds, would be more informative than a single discretization and set of thresholds.
483 For instance, SWE volume on 15 May 2015 was 10% less than the 36-year median 15 May SWE volume. However,
484 due to spring snowfall (Fig. 9), SWE volume on 30 May 2015 was 31% greater than the 36-year median on the same
485 date. Multiple discretizations could also be used to identify the locations of most (e.g., Fig. 4a and 4d) and least-
486 certain (Fig. 4b and 4c) opportunities for denning habitat. This information could be used as the basis for identifying
487 the locations where remote sensing or field campaigns could hone annual estimates of refugium, given that year's
488 meteorological conditions. Altogether, differences across discretizations (e.g., Fig. 6) and threshold sensitivities
489 (e.g., Fig. 9) could also be used to provide uncertainty bounds for PWDA calculated in any given year.

490 Our results show that caution is warranted when combining gridded data and static thresholds. While we focus on
491 the impact that thresholds and different snow spatial discretizations have on approximations of wolverine denning
492 opportunities, we expect these results to be applicable to other environmental applications. For instance, while
493 temperature thresholds are widely used to partition rain and snow precipitation in models, temperature discretized at
494 different spatial scales could influence the spatial variability of temperature and resulting snowfall volume
495 thresholded across one or many snowfall events (e.g., Jennings et al., 2018; Nolin and Daly, 2006; Wayand et al.,
496 2017). Snow cover thresholded using visible and infrared satellite observations may also require changes based on
497 the size of the satellite pixels and the underlying topographic and vegetative characteristics (Härer et al., 2018;

498 Pestana et al., 2019). Future studies should report the extent to which different spatial discretizations and ranges of
499 realistic thresholds influence results. This information could be used to report the 1) uncertainty of thresholded
500 outputs, 2) fidelity of different gridded products, and 3) the degree to which multiple spatial discretizations could be
501 combined to improve the fidelity and transferability of results.

6. Conclusions

503 Potential wolverine denning area (PWDA) was thresholded using a published SWE threshold (0.20 m) on a
504 threshold date (15 May) in a Colorado Rocky Mountain domain between 1985 and 2020. Results showed that
505 PWDA was statistically different ($p < 0.01$) between years with different winter precipitation magnitude (wet versus
506 dry) and precipitation temperature (cold versus warm) conditions. In fact, climate-driven differences in annual
507 PWDA were substantially larger than differences in PWDA between snow discretized using 1) discrete 480 m grid
508 cells, 2) 480 m grid cells with subgrid representations of SWE heterogeneity, and 3) discrete 90 m grid cells.
509 Therefore, studies that assess changes in habitat health for species like wolverines with past and future changes in
510 climate could be informative, regardless of the spatial discretizations tested.

511 Despite the sensitivity to winter climatic conditions, annual differences in denning patterns and parameter
512 sensitivities emerged for the different discretizations. For instance, 90 m grid cells resolved thinner snow deposits in
513 mid-to-upper elevations (approximately 3050 – 3350 m) that were not resolved by either of the 480 m
514 discretizations, decreasing PWDA by 10%, on average. Snow discretized with subgrid representations of SWE
515 spatial heterogeneity also had less-dramatic swings in annual PWDA. The simulations with subgrid SWE
516 heterogeneity increased PWDA by 10 – 30% in low-snow years, many of which were representative of future
517 changes in average temperature expected over the next 50 years. Spatially, the differences in the prevalence of SWE
518 that exceeded the threshold between the three different snow discretizations were heightened at the grid cells that
519 had SWE values close to the SWE threshold (0.20 m) on 15 May, the elevation of which was driven in large part by
520 the winter climatic conditions. On average, PWDA was more sensitive to the SWE threshold than the date threshold,
521 but had the smallest amount of sensitivity to the 480 m simulation with subgrid snow heterogeneity, which had more
522 gradual changes to the fraction of a region exceeding the SWE threshold with small changes in SWE. This
523 discretization also had the least amount of sensitivity to interannual changes in winter climatic conditions. However,
524 some years had late-spring snowfall events, altering the amount of PWDA by up to 82% depending on whether the
525 threshold date was before, during, or after the snowfall event.

526 Our results show that differences in how snow is spatially discretized can influence information generalized using
527 thresholds. Therefore, future studies thresholding spatiotemporal environmental data should include multiple spatial
528 discretizations and ranges of realistic thresholds to provide a more comprehensive picture of uncertainties associated
529 with chosen thresholds and datasets. Although we used wolverine habitat as an example, we expect these results to
530 be applicable to any study thresholding environmental data, especially for studies generalizing information at spatial
531 scales finer than those of modeled or observed resolutions.

Code and data availability

533 Readers are encouraged to enquire about the most up-to-date version of the reanalysis from the principal developer,
534 Steven Margulis. Scripts used in this manuscript are provided at https://github.com/jupflug/HABITAT-
535 threshold_vs_discretization.

Author contributions

537 JP and BL designed the experiments. YF and SM provided the snow reanalysis. JP wrote the manuscript, with
538 comments provided from all authors, and special supervision by BL.

Competing interests

540 The authors declare that they have no conflict of interest.

Support

542 This work was supported by the CIRES Visiting Fellows Program and the United States Geologic Survey (USGS)
543 award G21AC10645.

Acknowledgements

545 We would like to thank and acknowledge support from current and past U.S. Fish and Wildlife Service staff, in
546 particular, John Guinotte and Steve Torbit.

References

Araújo, M.B., Peterson, A.T., 2012. Uses and misuses of bioclimatic envelope modeling. Ecology 93, 1527–1539. https://doi.org/10.1890/11-1930.1

Auer, A.H., 1974. The Rain versus Snow Threshold Temperatures. Weatherwise 27, 67–67. https://doi.org/10.1080/00431672.1974.9931684

Barsugli, J.J., Ray, A.J., Livneh, B., Dewes, C.F., Heldmyer, A., Rangwala, I., Guinotte, J.M., Torbit, S., 2020. Projections of Mountain Snowpack Loss for Wolverine Denning Elevations in the Rocky Mountains. Earths Future 8, e2020EF001537. https://doi.org/10.1029/2020EF001537

Bernhardt, M., Schulz, K., 2010. SnowSlide: A simple routine for calculating gravitational snow transport. Geophys. Res. Lett. 37. https://doi.org/10.1029/2010GL043086

Boelman, N.T., Liston, G.E., Gurarie, E., Meddens, A.J.H., Mahoney, P.J., Kirchner, P.B., Bohrer, G., Brinkman, T.J., Cosgrove, C.L., Eitel, J.U.H., Hebblewhite, M., Kimball, J.S., LaPoint, S., Nolin, A.W., Pedersen, S.H., Prugh, L.R., Reinking, A.K., Vierling, L.A., 2019. Integrating snow science and wildlife ecology in Arctic-boreal North America. Environ. Res. Lett. 14, 010401. https://doi.org/10.1088/1748-9326/aaeec1

Bokhorst, S., Pedersen, S.H., Brucker, L., Anisimov, O., Bjerke, J.W., Brown, R.D., Ehrich, D., Essery, R.L.H., Heilig, A., Ingvander, S., Johansson, C., Johansson, M., Jónsdóttir, I.S., Inga, N., Luojus, K., Macelloni, G., Mariash, H., McLennan, D., Rosqvist, G.N., Sato, A., Savela, H., Schneebeli, M., Sokolov, A., Sokratov, S.A., Terzago, S., Vikhamar-Schuler, D., Williamson, S., Qiu, Y., Callaghan, T.V., 2016. Changing Arctic snow cover: A review of recent developments and assessment of future needs for observations, modelling, and impacts. Ambio 45, 516–537. https://doi.org/10.1007/s13280-016-0770-0

Cayan, D.R., 1996. Interannual Climate Variability and Snowpack in the Western United States. J. Clim. 9, 928–948. https://doi.org/10.1175/1520-0442(1996)009<0928:ICVASI>2.0.CO;2

Clark, M.P., Nijssen, B., Lundquist, J., Kavetski, D., Rupp, D.E., Woods, R.A., Freer, J.E., Gutmann, E.D., Wood, A.W., Brekke, L.D., Arnold, J.R., Gochis, D.J., Rasmussen, R.M., 2015. A unified approach for process-based hydrologic modeling: 1. Modeling concept. Water Resour. Res. 51, 2498–2514. https://doi.org/10.1002/2015WR017198

Copeland, J.P., McKelvey, K.S., Aubry, K.B., Landa, A., Persson, J., Inman, R.M., Krebs, J., Lofroth, E., Golden, H., Squires, J.R., Magoun, A., Schwartz, M.K., Wilmot, J., Copeland, C.L., Yates, R.E., Kojola, I., May, R., 2010. The bioclimatic envelope of the wolverine (Gulo gulo): do climatic constraints limit its geographic distribution? Can. J. Zool. 88, 233–246. https://doi.org/10.1139/Z09-136

Daloz, A.S., Mateling, M., L'Ecuyer, T., Kulie, M., Wood, N.B., Durand, M., Wrzesien, M., Stjern, C.W., Dimri, A.P., 2020. How much snow falls in the world's mountains? A first look at mountain snowfall estimates in A-train observations and reanalyses. The Cryosphere 14, 3195–3207. https://doi.org/10.5194/tc-14-3195-2020

Dierauer, J.R., Allen, D.M., Whitfield, P.H., 2019. Snow Drought Risk and Susceptibility in the Western United States and Southwestern Canada. Water Resour. Res. 55, 3076–3091. https://doi.org/10.1029/2018WR023229

Donald, J.R., Soulis, E.D., Kouwen, N., Pietroniro, A., 1995. A Land Cover-Based Snow Cover Representation for Distributed Hydrologic Models. Water Resour. Res. 31, 995–1009. https://doi.org/10.1029/94WR02973

Dozier, J., 1989. Spectral signature of alpine snow cover from the landsat thematic mapper. Remote Sens. Environ. 28, 9–22. https://doi.org/10.1016/0034-4257(89)90101-6

Durner, G.M., Simac, K., Amstrup, S.C., 2013. Mapping Polar Bear Maternal Denning Habitat in the National Petroleum Reserve — Alaska with an IfSAR Digital Terrain Model. Arctic 66, 197–206.

Egli, L., Jonas, T., Grünewald, T., Schirmer, M., Burlando, P., 2012. Dynamics of snow ablation in a small Alpine catchment observed by repeated terrestrial laser scans. Hydrol. Process. 26, 1574–1585.

Eyring, V., Bony, S., Meehl, G.A., Senior, C.A., Stevens, B., Stouffer, R.J., Taylor, K.E., 2016. Overview of the Coupled Model Intercomparison Project Phase 6 (CMIP6) experimental design and organization. Geosci. Model Dev. 9, 1937–1958. https://doi.org/10.5194/gmd-9-1937-2016

Feng, X., Sahoo, A., Arsenault, K., Houser, P., Luo, Y., Troy, T.J., 2008. The Impact of Snow Model Complexity at Three CLPX Sites. J. Hydrometeorol. 9, 1464–1481. https://doi.org/10.1175/2008JHM860.1

Gelaro, R., McCarty, W., Suárez, M.J., Todling, R., Molod, A., Takacs, L., Randles, C.A., Darmenov, A., Bosilovich, M.G., Reichle, R., Wargan, K., Coy, L., Cullather, R., Draper, C., Akella, S., Buchard, V., Conaty, A., Silva, A.M. da, Gu, W., Kim, G.-K., Koster, R., Lucchesi, R., Merkova, D., Nielsen, J.E., Partyka, G., Pawson, S., Putman, W., Rienecker, M., Schubert, S.D., Sienkiewicz, M., Zhao, B., 2017. The

Modern-Era Retrospective Analysis for Research and Applications, Version 2 (MERRA-2). J. Clim. 30, 5419–5454. https://doi.org/10.1175/JCLI-D-16-0758.1

Girotto, M., Margulis, S.A., Durand, M., 2014. Probabilistic SWE reanalysis as a generalization of deterministic SWE reconstruction techniques. Hydrol. Process. 28, 3875–3895. https://doi.org/10.1002/hyp.9887

Glass, T.W., Breed, G.A., Liston, G.E., Reinking, A.K., Robards, M.D., Kielland, K., 2021. Spatiotemporally variable snow properties drive habitat use of an Arctic mesopredator. Oecologia 195, 887–899. https://doi.org/10.1007/s00442-021-04890-2

Grünewald, T., Bühler, Y., Lehning, M., 2014. Elevation dependency of mountain snow depth. The Cryosphere 8, 2381–2394. https://doi.org/10.5194/tc-8-2381-2014

Hall, D.K., Riggs, G.A., 2007. Accuracy assessment of the MODIS snow products. Hydrol. Process. 21, 1534–1547. https://doi.org/10.1002/hyp.6715

Hamlet, A.F., Mote, P.W., Clark, M.P., Lettenmaier, D.P., 2005. Effects of Temperature and Precipitation Variability on Snowpack Trends in the Western United States. J. Clim. 18, 4545–4561. https://doi.org/10.1175/JCLI3538.1

Harder, P., Pomeroy, J., 2013. Estimating precipitation phase using a psychrometric energy balance method. Hydrol. Process. 27, 1901–1914. https://doi.org/10.1002/hyp.9799

Härer, S., Bernhardt, M., Siebers, M., Schulz, K., 2018. On the need for a time- and location-dependent estimation of the NDSI threshold value for reducing existing uncertainties in snow cover maps at different scales. The Cryosphere 12, 1629–1642. https://doi.org/10.5194/tc-12-1629-2018

Harpold, A., Dettinger, M., Rajagopal, S., 2017. Defining Snow Drought and Why It Matters. Eos. https://doi.org/10.1029/2017EO068775

He, S., Ohara, N., Miller, S.N., 2019. Understanding subgrid variability of snow depth at 1-km scale using Lidar measurements. Hydrol. Process. 33, 1525–1537. https://doi.org/10.1002/hyp.13415

Helbig, N., Bühler, Y., Eberhard, L., Deschamps-Berger, C., Gascoin, S., Dumont, M., Revuelto, J., Deems, J.S., Jonas, T., 2021. Fractional snow-covered area: scale-independent peak of winter parameterization. The Cryosphere 15, 615–632. https://doi.org/10.5194/tc-15-615-2021

Helbig, N., van Herwijnen, A., Magnusson, J., Jonas, T., 2015. Fractional snow-covered area parameterization over complex topography. Hydrol. Earth Syst. Sci. 19, 1339–1351. https://doi.org/10.5194/hess-19-1339-2015

Heldmyer, A.J., Bjarke, N.R., Livneh, B., 2023. A 21st-Century perspective on snow drought in the Upper Colorado River Basin. JAWRA J. Am. Water Resour. Assoc. 59, 396–415. https://doi.org/10.1111/1752-1688.13095

Herman, J.D., Giuliani, M., 2018. Policy tree optimization for threshold-based water resources management over multiple timescales. Environ. Model. Softw. 99, 39–51. https://doi.org/10.1016/j.envsoft.2017.09.016

Inman, R.M., Magoun, A.J., Persson, J., Mattisson, J., 2012. The wolverine's niche: linking reproductive chronology, caching, competition, and climate. J. Mammal. 93, 634–644. https://doi.org/10.1644/11-MAMM-A-319.1

Jennings, K.S., Winchell, T.S., Livneh, B., Molotch, N.P., 2018. Spatial variation of the rain–snow temperature threshold across the Northern Hemisphere. Nat. Commun. 9, 1148. https://doi.org/10.1038/s41467-018-03629-7

Jonas, T., Marty, C., Magnusson, J., 2009. Estimating the snow water equivalent from snow depth measurements in the Swiss Alps. J. Hydrol. 378, 161–167. https://doi.org/10.1016/j.jhydrol.2009.09.021

Kwadijk, J.C.J., Haasnoot, M., Mulder, J.P.M., Hoogvliet, M.M.C., Jeuken, A.B.M., van der Krogt, R.A.A., van Oostrom, N.G.C., Schelfhout, H.A., van Velzen, E.H., van Waveren, H., de Wit, M.J.M., 2010. Using adaptation tipping points to prepare for climate change and sea level rise: a case study in the Netherlands. WIREs Clim. Change 1, 729–740. https://doi.org/10.1002/wcc.64

Laliberte, A.S., Ripple, W.J., 2004. Range Contractions of North American Carnivores and Ungulates. BioScience 54, 123–138. https://doi.org/10.1641/0006-3568(2004)054[0123:RCONAC]2.0.CO;2

Liston, G.E., 2004. Representing Subgrid Snow Cover Heterogeneities in Regional and Global Models. J. Clim. 17, 1381–1397. https://doi.org/10.1175/1520-0442(2004)017<1381:RSSCHI>2.0.CO;2

Liston, G.E., Elder, K., 2006. A Distributed Snow-Evolution Modeling System (SnowModel). J. Hydrometeorol. 7, 1259–1276. https://doi.org/10.1175/JHM548.1

Liston, G.E., Perham, C.J., Shideler, R.T., Cheuvront, A.N., 2016. Modeling snowdrift habitat for polar bear dens. Ecol. Model. 320, 114–134. https://doi.org/10.1016/j.ecolmodel.2015.09.010

Liu, Y., Margulis, S.A., 2019. Deriving Bias and Uncertainty in MERRA-2 Snowfall Precipitation Over High Mountain Asia. Front. Earth Sci. 7. https://doi.org/10.3389/feart.2019.00280

655 Livneh, B., Deems, J.S., Schneider, D., Barsugli, J.J., Molotch, N.P., 2014. Filling in the gaps: Inferring spatially
656   distributed precipitation from gauge observations over complex terrain. Water Resour. Res. 50, 8589–8610.
657   https://doi.org/10.1002/2014WR015442
658 Luce, C.H., Tarboton, D.G., Cooley, K.R., 1998. The influence of the spatial distribution of snow on basin-averaged
659   snowmelt. Hydrol. Process. 12, 1671–1683. https://doi.org/10.1002/(SICI)1099-
660   1085(199808/09)12:10/11<1671::AID-HYP688>3.0.CO;2-N
661 Lundquist, J.D., Dettinger, M.D., 2005. How snowpack heterogeneity affects diurnal streamflow timing. Water
662   Resour. Res. 41. https://doi.org/10.1029/2004WR003649
663 Machguth, H., Paul, F., Hoelzle, M., Haeberli, W., 2006. Distributed glacier mass-balance modelling as an
664   important component of modern multi-level glacier monitoring. Ann. Glaciol. 43, 335–343.
665   https://doi.org/10.3189/172756406781812285
666 Magoun, A.J., Robards, M.D., Packila, M.L., Glass, T.W., 2017. Detecting snow at the den-site scale in wolverine
667   denning habitat. Wildl. Soc. Bull. 41, 381–387. https://doi.org/10.1002/wsb.765
668 Maher, A.I., Treitz, P.M., Ferguson, M.A.D., 2012. Can Landsat data detect variations in snow cover within habitats
669   of arctic ungulates? Wildl. Biol. 18, 75–87. https://doi.org/10.2981/11-055
670 Mahoney, P.J., Liston, G.E., LaPoint, S., Gurarie, E., Mangipane, B., Wells, A.G., Brinkman, T.J., Eitel, J.U.H.,
671   Hebblewhite, M., Nolin, A.W., Boelman, N., Prugh, L.R., 2018. Navigating snowscapes: scale-dependent
672   responses of mountain sheep to snowpack properties. Ecol. Appl. 28, 1715–1729.
673   https://doi.org/10.1002/eap.1773
674 Margulis, S.A., Cortés, G., Girotto, M., Durand, M., 2016. A Landsat-Era Sierra Nevada Snow Reanalysis (1985–
675   2015). J. Hydrometeorol. 17, 1203–1221. https://doi.org/10.1175/JHM-D-15-0177.1
676 Margulis, S.A., Girotto, M., Cortés, G., Durand, M., 2015. A Particle Batch Smoother Approach to Snow Water
677   Equivalent Estimation. J. Hydrometeorol. 16, 1752–1772. https://doi.org/10.1175/JHM-D-14-0177.1
678 Margulis, S.A., Liu, Y., Baldo, E., 2019. A Joint Landsat- and MODIS-Based Reanalysis Approach for Midlatitude
679   Montane Seasonal Snow Characterization. Front. Earth Sci. 7. https://doi.org/10.3389/feart.2019.00272
680 McKelvey, K.S., Copeland, J.P., Schwartz, M.K., Littell, J.S., Aubry, K.B., Squires, J.R., Parks, S.A., Elsner, M.M.,
681   Mauger, G.S., 2011. Climate change predicted to shift wolverine distributions, connectivity, and dispersal
682   corridors. Ecol. Appl. 21, 2882–2897. https://doi.org/10.1890/10-2206.1
683 Mendoza, P.A., Musselman, K.N., Revuelto, J., Deems, J.S., López-Moreno, J.I., McPhee, J., 2020. Interannual and
684   Seasonal Variability of Snow Depth Scaling Behavior in a Subalpine Catchment. Water Resour. Res. 56,
685   e2020WR027343. https://doi.org/10.1029/2020WR027343
686 Mote, P.W., Hamlet, A.F., Clark, M.P., Lettenmaier, D.P., 2005. DECLINING MOUNTAIN SNOWPACK IN
687   WESTERN NORTH AMERICA*. Bull. Am. Meteorol. Soc. 86, 39–50. https://doi.org/10.1175/BAMS-86-
688   1-39
689 Nolin, A.W., Daly, C., 2006. Mapping "at risk" snow in the Pacific Northwest. J. Hydrometeorol. 7, 1164–1171.
690 Pestana, S., Chickadel, C.C., Harpold, A., Kostadinov, T.S., Pai, H., Tyler, S., Webster, C., Lundquist, J.D., 2019.
691   Bias Correction of Airborne Thermal Infrared Observations Over Forests Using Melting Snow. Water
692   Resour. Res. 55, 11331–11343. https://doi.org/10.1029/2019WR025699
693 Pflug, J.M., Hughes, M., Lundquist, J.D., 2021. Downscaling snow deposition using historic snow depth patterns:
694   Diagnosing limitations from snowfall biases, winter snow losses, and interannual snow pattern
695   repeatability. Water Resour. Res. e2021WR029999. https://doi.org/10.1029/2021WR029999
696 Pflug, J.M., Liston, G.E., Nijssen, B., Lundquist, J.D., 2019. Testing Model Representations of Snowpack Liquid
697   Water Percolation Across Multiple Climates. Water Resour. Res. 55, 4820–4838.
698   https://doi.org/10.1029/2018WR024632
699 Pflug, J.M., Lundquist, J.D., 2020. Inferring Distributed Snow Depth by Leveraging Snow Pattern Repeatability:
700   Investigation Using 47 Lidar Observations in the Tuolumne Watershed, Sierra Nevada, California. Water
701   Resour. Res. 56, e2020WR027243. https://doi.org/10.1029/2020WR027243
702 Pflug, J.M., Margulis, S.A., Lundquist, J.D., 2022. Inferring watershed-scale mean snowfall magnitude and
703   distribution using multidecadal snow reanalysis patterns and snow pillow observations. Hydrol. Process.
704   36, e14581. https://doi.org/10.1002/hyp.14581
705 Ray, A.L., Barsugli, J.J., Livneh, B., Dewes, C.F., Rangwala, I., Heldmyer, A., Stewart, J., 2017. Future Snow
706   Persistence in Rocky Mountain and Glacier National Parks: An Analysis to Inform the USFWS Wolverine
707   Species Status Assessment. NOAA/ESRL/Physical Sciences Division, CU/Cooperative Institute for
708   Research in Environmental Sciences (CIRES), and CU Civil, Environmental & Architectural Engineering.

709 Sankey, T., Donald, J., McVay, J., Ashley, M., O'Donnell, F., Lopez, S.M., Springer, A., 2015. Multi-scale analysis
710   of snow dynamics at the southern margin of the North American continental snow distribution. Remote
711   Sens. Environ. 169, 307–319. https://doi.org/10.1016/j.rse.2015.08.028
712 Scott, J.D., Alexander, M.A., Murray, D.R., Swales, D., Eischeid, J., 2016. The Climate Change Web Portal: A
713   System to Access and Display Climate and Earth System Model Output from the CMIP5 Archive. Bull.
714   Am. Meteorol. Soc. 97, 523–530. https://doi.org/10.1175/BAMS-D-15-00035.1
715 Serreze, M.C., Clark, M.P., Armstrong, R.L., McGinnis, D.A., Pulwarty, R.S., 1999. Characteristics of the western
716   United States snowpack from snowpack telemetry (SNOTEL) data. Water Resour. Res. 35, 2145–2160.
717   https://doi.org/10.1029/1999WR900090
718 Shih, J.-S., ReVelle, C., 1995. Water supply operations during drought: A discrete hedging rule. Eur. J. Oper. Res.
719   82, 163–175. https://doi.org/10.1016/0377-2217(93)E0237-R
720 Sivy, K.J., Nolin, A.W., Cosgrove, C.L., Prugh, L.R., 2018. Critical snow density threshold for Dall's sheep (Ovis
721   dalli dalli). Can. J. Zool. 96, 1170–1177. https://doi.org/10.1139/cjz-2017-0259
722 Skaugen, T., Melvold, K., 2019. Modeling the Snow Depth Variability With a High-Resolution Lidar Data Set and
723   Nonlinear Terrain Dependency. Water Resour. Res. 55, 9689–9704.
724   https://doi.org/10.1029/2019WR025030
725 USFWS, 2018. Species status assessment report for the North American Wolverine (Gulo gulo luscus). (No. Version
726   1.2.). U.S. Fish and Wildlife Service, Mountain-Prarie Region, Lakewood, CO.
727 Vögeli, C., Lehning, M., Wever, N., Bavay, M., 2016. Scaling Precipitation Input to Spatially Distributed
728   Hydrological Models by Measured Snow Distribution. Front. Earth Sci. 4.
729   https://doi.org/10.3389/feart.2016.00108
730 Wayand, N.E., Clark, M.P., Lundquist, J.D., 2017. Diagnosing snow accumulation errors in a rain-snow transitional
731   environment with snow board observations. Hydrol. Process. 31, 349–363.
732   https://doi.org/10.1002/hyp.11002
733 Wigmosta, M.S., Nijssen, B., Storck, P., Lettenmaier, D.P., 2002. The distributed hydrology soil vegetation model.
734   Math. Models Small Watershed Hydrol. Appl. 7–42.
735 Xiao, M., Mahanama, S.P., Xue, Y., Chen, F., Lettenmaier, D.P., 2021. Modeling Snow Ablation over the
736   Mountains of the Western United States: Patterns and Controlling Factors. J. Hydrometeor. 22, 297–311.
737   https://doi.org/10.1175/JHM-D-19-0198.1
738 Xue, Y., Sellers, P.J., Kinter, J.L., Shukla, J., 1991. A Simplified Biosphere Model for Global Climate Studies. J.
739   Clim. 4, 345–364. https://doi.org/10.1175/1520-0442(1991)004<0345:ASBMFG>2.0.CO;2
740 Yang, K., Musselman, K.N., Rittger, K., Margulis, S.A., Painter, T.H., Molotch, N.P., 2021. Combining ground-
741   based and remotely sensed snow data in a linear regression model for real-time estimation of snow water
742   equivalent. Adv. Water Resour. 104075. https://doi.org/10.1016/j.advwatres.2021.104075
743